ACCOUNTS
of chemical research

Redox Deposition of Nanoscale Metal Oxides on Carbon for Next-Generation Electrochemical Capacitors

MEGAN B. SASSIN, CHRISTOPHER N. CHERVIN,
DEBRA R. ROLISON, AND JEFFREY W. LONG*
U.S. Naval Research Laboratory, Surface Chemistry Branch (Code 6170), Washington, D.C. 20375, United States

RECEIVED ON OCTOBER 26, 2011

CONSPECTUS

Transition metal oxides that mix electronic and ionic conductivity are essential active components of many electrochemical charge-storage devices, ranging from primary alkaline cells to more advanced rechargeable Li-ion batteries. In these devices, charge storage occurs via cation-insertion/deinsertion mechanisms in conjunction with the reduction/oxidation of metal sites in the oxide. Batteries that incorporate such metal oxides are typically designed for high specific energy, but not necessarily for high specific power. Electrochemical capacitors (ECs), which are typically composed of symmetric high-surface-area carbon electrodes that store charge via double-layer capacitance, deliver their energy in time scales of seconds, but at much lower specific energy than batteries. The fast, reversible faradaic reactions (typically described as "pseudocapacitance") of particular nanoscale metal oxides (e.g., ruthenium and manganese oxides) provide a strategy for bridging the power/energy performance gap between batteries and conventional ECs. These processes enhance charge-storage capacity to boost specific energy, while maintaining the few-second timescale of the charge–discharge response of carbon-based ECs.

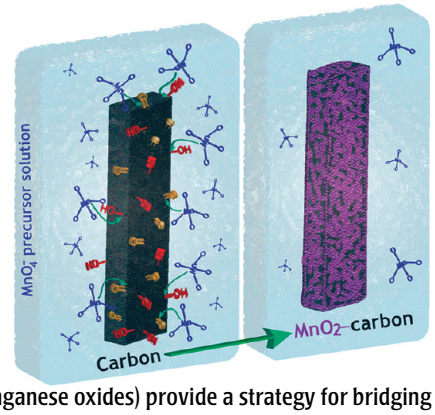

In this Account, we describe three examples of redox-based deposition of EC-relevant metal oxides (MnO_2, FeO*x*, and RuO_2) and discuss their potential deployment in next-generation ECs that use aqueous electrolytes. To extract the maximum pseudocapacitance functionality of metal oxides, one must carefully consider how they are synthesized and subsequently integrated into practical electrode structures. Expressing the metal oxide in a nanoscale form often enhances electrochemical utilization (maximizing specific capacitance) and facilitates high-rate operation for both charge and discharge. The "wiring" of the metal oxide, in terms of both electron and ion transport, when fabricated into a practical electrode architecture, is also a critical design parameter for achieving characteristic EC charge–discharge timescales. For example, conductive carbon must often be combined with the poorly conductive metal oxides to provide long-range electron pathways through the electrode. However, the ad hoc mixing of discrete carbon and oxide powders into composite electrodes may not support optimal utilization or rate performance. As an alternative, nanoscale metal oxides of interest for ECs can be synthesized directly on the surfaces of nanostructured carbons, with the carbon surface acting as a sacrificial reductant when exposed to a solution-phase, oxidizing precursor of the desired metal oxide (e.g., MnO_4^- for MnO_2). These redox deposition methods can be applied to advanced carbon nanoarchitectures with well-designed pore structures. These architectures promote effective electrolyte infiltration and ion transport to the nanoscale metal oxide domains within the electrode architecture, which further enhances high-rate operation.

Introduction

When a burst of energy must be delivered on the time scale of seconds (10^{-1}–10^{2} s), batteries miss the power delivery window while electrostatic capacitors expend their energy in microseconds to milliseconds and have nothing left to give. Electrochemical capacitors (ECs, also denoted as "ultracapacitors" and "supercapacitors") fill a temporal performance void that is critical for recapturing waste energy (e.g., from braking in an electric or gas/electric hybrid vehicle) or providing energy bursts for portable communication

Published on the Web 03/01/2012 www.pubs.acs.org/accounts
10.1021/ar2002717

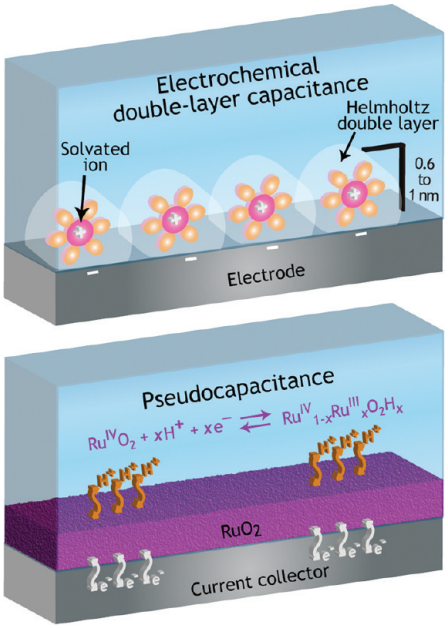

FIGURE 1. Schematic of charge storage via electrochemical double-layer capacitance and pseudocapacitance.

devices.[1,2] The few-seconds time scale over which energy is released from ECs serves as one performance criterion; another is the magnitude of the energy released during the desired pulse of power. Many present and foreseen applications require more energy to be delivered in seconds than can be achieved with EDLCs (electric double-layer capacitors), which store charge in the electric double-layer (Figure 1) and are characterized by relatively low specific energy (3–8 versus >100 W h kg^{-1} for Li-ion batteries), even using high-surface-area carbon electrodes.[3,4]

To increase the specific energy released by ECs, researchers are turning to an additional charge-storage mechanism—pseudocapacitance, or a double insertion of an electron and cation (either protons or supporting electrolyte cations, such as Na^+ or K^+) into a mixed electron/ion conductive material (Figure 1).[5–7] Transition metal oxides, such as RuO_2 and MnO_2, are prime candidates as the pseudocapacitive phase, particularly when used in aqueous-electrolyte ECs.[8–12] The main drawback to the use of most metal oxides is that their limited electronic conductivity restricts power delivery on the few-seconds time scale. The traditional workaround is to mix the active oxide with carbon powder into a composite electrode, not unlike the approach used to form electrodes for batteries, but the ad-hoc nature of the powder-composite electrode structure potentially precludes a high-rate response.

A more design-rich strategy is to move toward advanced composites and architectures,[13] particularly those in which

TABLE 1. Oxidation Potentials of Select Metal-Oxide Precursors

oxidant	oxidation potential, acidic	oxidation potential, alkaline
MnO_4^-	1.67	0.56
FeO_4^{2-}	2.20	0.72
RuO_4^{2-}		−0.22
RuO_4^-		0.59
RuO_4		1.0

the pseudocapacitive metal oxide is more intimately associated with nanostructured carbon substrates. The electrochemical utilization of such rewired metal oxides can be significantly enhanced when expressed as nanoscale films, as shown for ultrathin MnO_2 (tens to hundreds of nm), with specific capacitances approaching the theoretical value of 1370 F g^{-1} for storing one electron per Mn center,[14,15] as compared to conventional powder-composite electrodes of MnO_2, where the capacitance rarely exceeds 200 F g^{-1}.[16] The properties of thin-film metal oxides can be translated to more practical electrode and device size regimes by incorporating the metal oxide as a nanoscale coating on conductive carbon supports. Many protocols, including electrodeposition,[17] vapor deposition,[18] impregnation/decomposition,[19] and sol–gel chemistry[20] have been used to synthesize such metal oxide–carbon nanomaterials, but not all methods yield conformal coatings on nanostructured surfaces, and optimized contact between metal oxide and carbon is not necessarily achieved.

Redox deposition of metal oxides, as achieved by reacting the corresponding strong-oxidant precursor (MnO_4^-, FeO_4^{2-}, RuO_4; Table 1) at the surface of carbon (acting as reductant), offers an attractive alternative in terms of scalability, cost, and manufacturability.[21] Although a seemingly simple deposition protocol (exposing the desired carbon substrate to a solution of the oxidant), it is often necessary to tune reaction conditions in order to promote maximum metal-oxide loading while also maintaining conformality of the deposit. We find that when conditions that ensure self-limiting deposition are attained, we preserve the complex pore structures of mesoporous (2–50 nm pores) and macroporous (>50 nm pores) carbon substrates (Figure 2), thereby enabling facile electrolyte infiltration and high-rate electrochemical performance.[22–24] In the following sections, we describe specific examples of redox deposition of MnO_2, FeO*x*, and RuO_2 on a variety of nanostructured carbon substrates and the implications of composition and architecture when the resulting metal oxide–carbon electrode structures are used as charge-storing architectures for aqueous ECs.

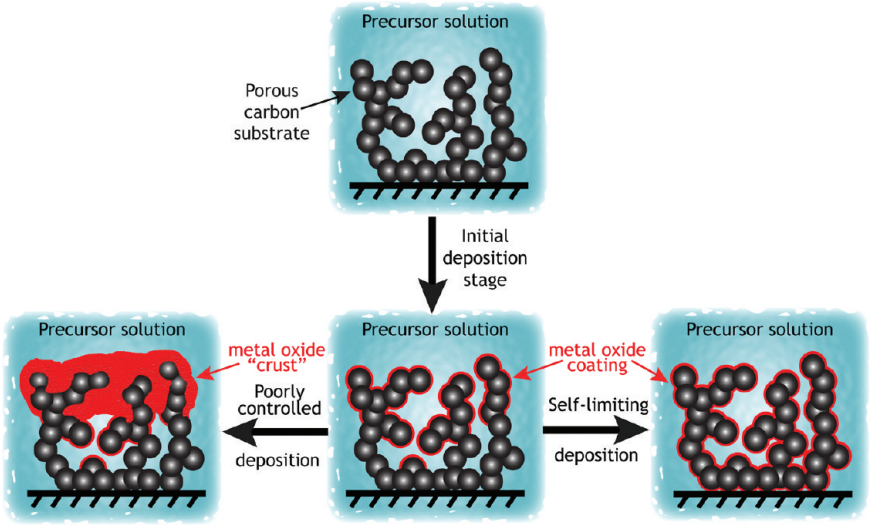

FIGURE 2. Schematic of redox deposition under "poorly controlled" (left) versus "self-limiting" (right) conditions.

Redox Deposition Approaches to Nanoscale Coatings of Metal Oxides

Manganese Oxides. Permanganate (MnO_4^-) is a versatile, readily available, and water-soluble oxidizing agent commonly used in organic synthesis,[25] wastewater treatment,[26] and can serve as a precursor to MnO_2 upon reaction with an appropriate reducing agent (e.g., Mn^{2+}, sugars, alcohols, unsaturated organic acids).[27,28] While permanganate has long been used to oxidize carbon surfaces to enhance electrochemical performance, Chen and co-workers were the first to recognize the simplicity and scalability of the permanganate–carbon redox reaction for generating MnO*x* coatings that store charge.[21] The initial study performed on planar graphite had limited utility for real-world ECs because of the small quantity of charge stored, but as the authors predicted, redox deposition can be extended to more EC-relevant high-surface-area and 3D carbon substrates, including carbon blacks,[29,30] templated mesoporous carbon,[31−34] nanotubes,[35−40] graphene,[41,42] and nanofoams.[22,23]

Ma and co-workers posited that the reaction of permanganate with acetylene black (AB) begins as protons adsorb at the carbon surface from the aqueous permanganate solution (pH∼5),[29,35] evidenced by a sharp increase in solution pH and a decrease in solution potential (Figure 3). The interfacial localization of protons from solution and electrons from the carbon substrate favors the reduction of permanganate to a mixed-valent manganese (III/IV) oxide, designated as MnO_2, according to the equation

$$MnO_4^- + 4H^+ + 3e^- \rightarrow MnO_2 + 2H_2O \qquad (1)$$

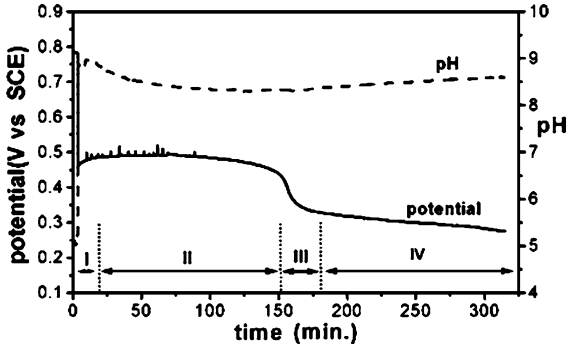

FIGURE 3. Electrode potential and pH versus time for reaction of $KMnO_4$ with acetylene black. Reprinted with permission from ref 29. Copyright 2006 The Electrochemical Society.

Later studies showed that CO_2 is generated as a byproduct, confirming a direct reaction between permanganate and AB.[30]

$$4MnO_4^- + 3C + 2H_2O \rightarrow 4MnO_2 + 3CO_2 + 4OH^- \qquad (2)$$

A more complex reaction scheme is proposed for multiwalled carbon nanotubes (CNTs) with oxidation occurring primarily at edge-plane sites or other defects; MnO_2 deposition initiates at these defects and then propagates to other surface sites, coupled to electron transport through the nanotubes (Figure 4).[35]

Permanganate reduction at carbon is influenced by such factors as temperature, pH, concentration, and the functionality of the carbon surface. Acidic solutions are used to accelerate the reaction or to modify carbon surfaces that are more resistant to oxidation (e.g., the basal-plane surfaces predominant in CNTs). Faster MnO_2-deposition rates

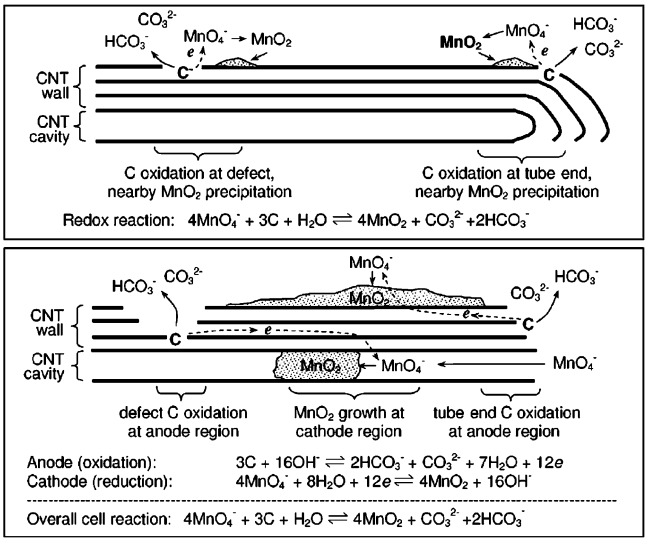

FIGURE 4. Schematic of redox deposition of MnO_2 on CNTs at initial and later stages. Reprinted with permission from ref 35. Copyright 2007 Wiley InterScience.

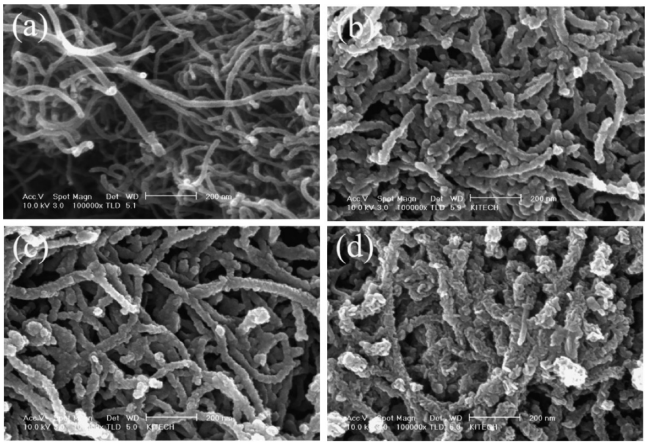

FIGURE 5. Scanning electron microscopy images of (a) pristine CNTs, and MnO_2-coated CNTs prepared from (b) pH 7, (c) pH 2.5, and (d) pH 1 $KMnO_4$ solution. Reprinted with permission from ref 36. Copyright 2007 Elsevier.

at CNTs occur at pH 1 compared to permanganate solutions at pH 2.5 and 7; conformal, nanoscale MnO_2 coating are achieved at all pHs, but surface morphologies were rougher for deposition at pH 1 (Figure 5).[36] The sp^2 character of pristine CNT and graphene surfaces makes them difficult to oxidize, and thus additional measures, such as conventional heating (70−140 °C)[37] or microwave irradiation,[41] may be required to drive the permanganate−carbon reaction. Alternatively, CNTs and graphene may be first preoxidized with strong acid to make them more amenable to a subsequent permanganate−carbon reaction step to generate the desired MnO_2 coating.[35,38−40,42]

Acidic conditions not only enhance the permanganate−carbon reaction rate, but also the competing autocatalytic decomposition of permanganate (via oxidation of H_2O).[43] Fischer and co-workers demonstrated the importance of avoiding acidic deposition conditions when modifying prefabricated, macroscale forms of an ultraporous carbon substrate (e.g., 170 μm thick carbon nanofoam papers),[22,23] as opposed to dispersions of carbon powders. Under acidic conditions, micrometers-thick MnO_2 coatings form at the exterior of carbon nanofoam paper (Figure 6a,b), occluding the pore structure and frustrating MnO_2 deposition within the interior void volume. These thick crusts of poorly conductive MnO_2 also impose an undesirable charge-transfer resistance to the resulting electrode structure (Figure 7a), markedly limiting EC performance. Under neutral-pH conditions, autocatalytic permanganate decomposition is suppressed and the permanganate−carbon reaction self-limits, resulting in nanoscale (~10 nm thick) MnO_2 coatings that conform to the carbon walls throughout the nanofoam paper (Figure 6c,d), enhance electrode capacitance, and maintain the frequency response of the native carbon nanofoam (Figure 7b).

The thickness, conformality, distribution, and weight loading of the MnO_2 coating depend not only on the deposition conditions but also on the nature of the nanostructured carbon substrate; the interplay of these design features ultimately determines the electrochemical performance of the resulting MnO_2-modified carbon. Dong et al. showed that reaction at short times between dilute permanganate and templated mesoporous carbons (ordered 3−5 nm pores) yields nanoscopic MnO_2 embedded into the carbon walls.[31] When cycled in aqueous 2 M KCl, the resulting MnO_2-modified carbons demonstrated enhanced total electrode capacitance (173 versus 105 F g^{-1} for the native carbon) and high MnO_2 utilization (628 F $g_{(MnO_2)}{}^{-1}$) at a relatively low weight loading (13 wt % MnO_2); with this protocol, diminishing returns in utilization were observed as the weight loading increased to a maximum of 26 wt % MnO_2.[32] Peng et al. used a hierarchical pore structure comprising distinct, but interconnected, networks of mesopores (6−8 nm) and macropores (70−100 nm) to improve on the limited MnO_2 uptake of templated carbons that are strictly mesoporous.[34] Oxide loadings as high as 83 wt % were achieved, but at the expense of clogging the mesopore channels, which in turn, inhibited electrolyte infiltration, and resulted in lower total specific capacitance (166 F g^{-1} with 80 % with 80 % active MnO_2−carbon material) than observed at much lower MnO_2 loadings with the mesoporous carbon substrates.

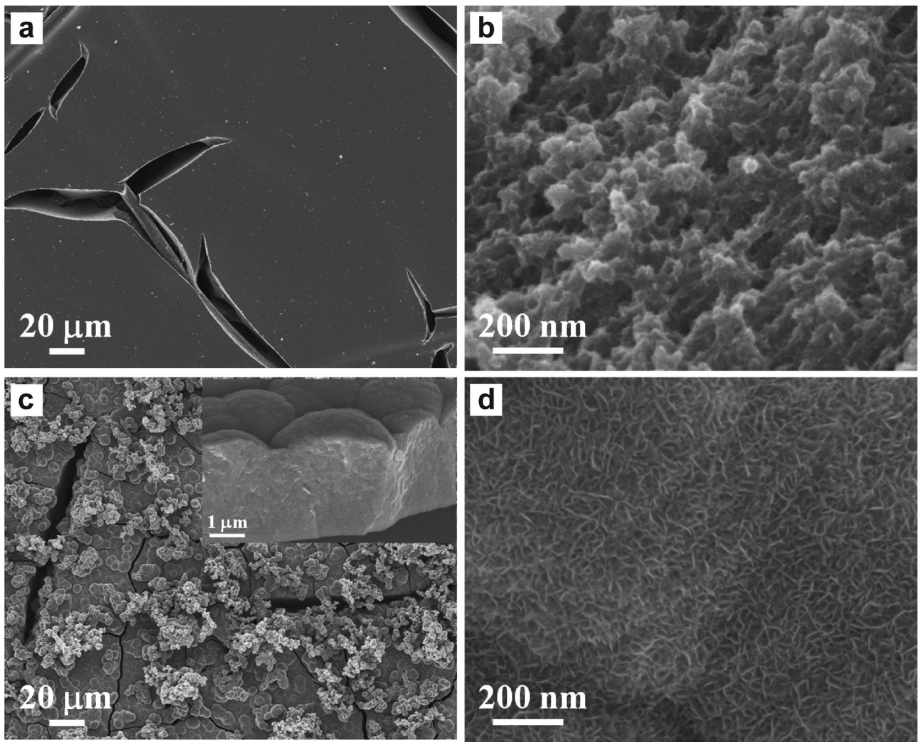

FIGURE 6. Micrographs of (a,b) acid-deposited and (c,d) neutral-deposited MnO_2–carbon nanofoams. Adapted with permission from ref 22. Copyright 2007 American Chemical Society.

Yan et al. achieved similarly high MnO_2 weight loadings (78 wt %) on graphene, but with better electrochemical utilization, as evidenced by a specific capacitance of 310 F g^{-1} (normalized to MnO_2–graphene). The enhanced capacitance on graphene substrates may arise from their higher electronic conductivity, which also supports performance at high charge–discharge rates.[41] The effect of the carbon substrate was also explored by Chu et al., who demonstrated higher specific capacitance (208 F g^{-1}) and lower electrode resistance (19 Ω) when MnO_2 was deposited onto CNTs versus an AB substrate with similar MnO_2 loading (63 wt % versus 69 wt % for the CNT), but which provided only 158 F g^{-1} and higher resistance (28 Ω).[37]

The earliest examples of MnO_2-based electrodes for ECs were fabricated by mixing MnO_2 powders with carbon powders and polymer binder to form a composite electrode,[16] which, although simple and scalable, hinders high-rate performance due to limited electronic contact between conductive carbon and micrometer-sized particles of the poorly conductive MnO_2 (Figure 8, top). The permanganate–carbon reaction promotes intimate contact between the MnO_2 and carbon components that improves electrochemical performance, but the full benefits of such MnO_2–carbon materials are not realized when processed into conventional powder-composite electrodes (Figure 8, middle), due to the following complications: (i) active MnO_2 sites may become obscured when mixed with binder and other additives; (ii) long-range electron-conducting pathways (the carbon component) may be disrupted in the ad hoc mixture of powdered components; and (iii) poorly interconnected void volume may frustrate electrolyte infiltration. A more desirable design would begin with a macroscale, preformed carbon scaffold onto which nanoscale coatings of MnO_2 are deposited (Figure 8, bottom). The proposed electrode design would be device-ready, provide control over pore–solid architecture via the choice of carbon substrate, maintain uninterrupted electron-conducting pathways throughout the macroscale carbon scaffold, and establish a desired frequency response.

In one such example, CNTs are first applied to the fibers comprising a carbon fiber paper (CFP) to create a free-standing architecture with micrometer-sized voids; subsequent reaction with permanganate deposits nanoscale MnO_2 at the CNTs.[39] The free-standing MnO_2–CNT–CFP electrode exhibited 322 F $g_{(MnO_2)}^{-1}$ in 0.65 M K_2SO_4 at 1 mV s^{-1} that decreased to 219 F $g_{(MnO_2)}^{-1}$ at 5 mV s^{-1}. The voltammograms were rectangular in shape and did not exhibit significant resistance even at 200 mV s^{-1}, which is not surprising considering the large open void network of the CFP and the relatively low loading of MnO_2 (0.15 mg cm^{-2}

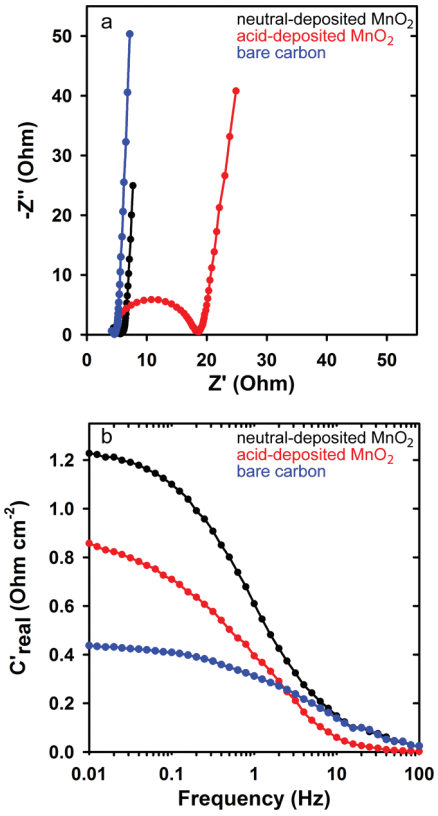

FIGURE 7. (a) Nyquist and (b) Bode plots of bare carbon (blue), acid-deposited (red), and neutral deposited MnO_2–carbon (black) at 0.2V versus SCE in 1 M Na_2SO_4. Adapted with permission from ref 22. Copyright 2007 American Chemical Society.

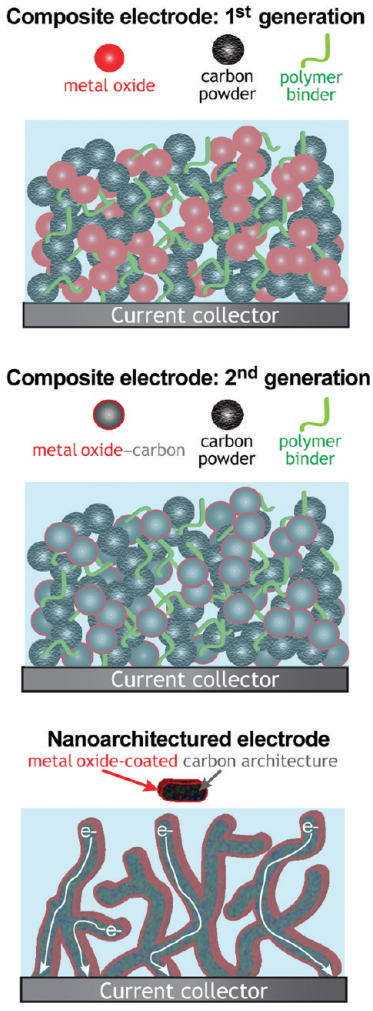

FIGURE 8. Schematic of electrolyte-infiltrated electrode structures incorporating electron paths, active, and inactive materials, using composites, versus a nanoarchitecture incorporating electron paths wired to the active material.

geometric area). Although the rate capabilities of this composite are impressive, the low MnO_2 loading and high fraction of void volume (in the large spaces between carbon fibers) limits the mass- and volume-normalized capacitance that can be achieved.[39]

The high fraction of void volume in CFP can be more optimally used by filling with a sol–gel-derived polymer precursor (resorcinol–formaldehyde, RF) followed by carbonization to yield a device-ready carbon nanofoam paper that exhibits high specific surface area (200–600 $m^2\ g^{-1}$), electronic conductivity (10–200 $S\ cm^{-1}$), a through-connected network of size-tunable pores (10 nm to a few μm), and scalability in both thickness (70–300 μm) and geometric footprint (~100 cm^2).[44,45] The resulting pyrolytic carbon readily reacts with permanganate at room temperature to produce nanoscale conformal MnO_2 coatings throughout the thickness of the nanofoam.[22,23] These first examples, using a commercially available carbon nanofoam paper, demonstrated a MnO_2 weight uptake of 37 wt % and a concomitant enhancement in total electrode capacitance from 53 to 140 $F\ g^{-1}$, with a MnO_2-normalized capacitance of 350 $F\ g^{-1}$. While the increase in specific capacitance is promising, even greater enhancements in volumetric and geometric capacitance (factor of 10) are achieved because the conformal, nanoscale MnO_2 coating does not increase the electrode volume or footprint.

The MnO_2 weight loadings and corresponding electrochemical performance metrics can be further enhanced by fine-tuning the pore structure and macroscale thickness of the carbon nanofoam electrode structure.[45] By selecting an RF formulation that yields higher specific surface area, one can increase the MnO_2 loading and improve mass- and volume-normalized capacitance (up to 200 $F\ cm^{-3}$). The geometric capacitance (electrode footprint normalized) for MnO_2-modified nanofoams scales from 2.5 $F\ cm^{-2}$ for a 70 μm thick nanofoam to 5.0 and 7.5 $F\ cm^{-2}$ for 120 and 230 μm thick nanofoams, respectively (Figure 9), confirming

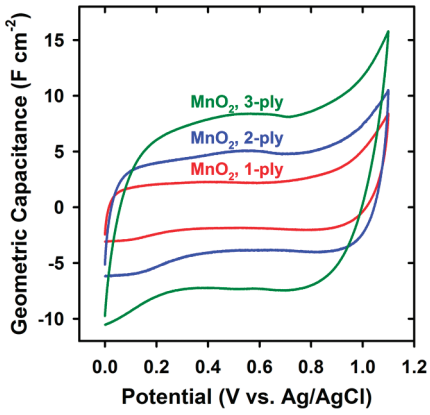

FIGURE 9. Geometric capacitance versus potential of 1-ply (red), 2-ply (blue), and 3-ply (green) MnO_2–carbon nanofoam electrodes in 2.5 M Li_2SO_4 at 5 mVs^{-1}. Adapted with permission from ref 45. Copyright 2011 Royal Society of Chemistry.

that MnO_2 not only deposits throughout the full thickness of the paper but is electrochemically accessible.[45]

Iron Oxide. Ferrate (FeO_4^{2-}) is a close relative of permanganate and has been used for similar applications, such as wastewater treatment.[46] Mao et al. demonstrated that reaction with ferrate introduces oxygen functionalities on the surfaces of graphite, which enhances reversible capacity and cycling stability when used as a negative electrode for Li-ion batteries, although the resulting FeO*x* deposit was removed prior to use.[47] Less frequently studied than other transition metal oxides, FeO*x* can also serve as an active material for electrochemical charge storage, for example as a negative electrode material for aqueous asymmetric ECs.[48] We were the first to report that reaction of ferrate with carbon substrates (e.g., carbon nanofoam papers) generates electrochemically active FeO*x* coatings.[24]

Although ferrate–carbon and permanganate–carbon reactions are similar in mechanism, ferrate-based depositions are more challenging because ferrate solutions are only stable in a narrow alkaline-pH range (~7–10 M KOH), have limited shelf life (hours to days), and their high viscosity impedes infiltration into the void volume of the carbon substrate. With appropriate deposition conditions (e.g., using 25 mM K_2FeO_4 in 9 M KOH), self-limiting, nanoscale FeO*x* coatings are generated at the inner and outer surfaces of carbon nanofoam papers while retaining the through-connected pore structure of the native nanofoam (Figures 10 and 11). The weight loading of FeO*x* is primarily controlled by the pore structure of the native carbon nanofoam (Table 2 and Figure 11), where smaller mesopores (<20 nm) limit FeO*x* incorporation despite higher specific surface area compared to nanofoams with larger mesopores (20–50 nm) and/or small macropores (50–100 nm). This trend reflects the fact that more facile infusion of the viscous ferrate solution into the architecture occurs as pore size increases.

When FeO*x*–carbon nanofoams are electrochemically cycled in mild aqueous electrolytes, they exhibit enhanced charge storage via faradaic pseudocapacitance that is proportional to the FeO*x* loading (Table 2 and Figure 11).[24] The FeO*x*-normalized capacitances of such electrode architectures (>300 F $g_{(FeOx)}^{-1}$) exceed those previously reported (typically <120 F $g_{(FeOx)}^{-1}$) for both thin-films and powder-composites,[49,50] demonstrating greater electrochemical utilization when the FeO*x* is intimately associated with a well-designed carbon substrate (Figure 10c,d). The FeO*x* pseudocapacitance arises from reversibly toggling the average Fe oxidation state between 3.0 and 2.7, as verified by X-ray absorption spectroscopy analysis of the FeO*x*–carbon nanofoam under electrochemical control.[24] The electrochemical stability of the FeO*x* coating is highly dependent on electrolyte pH; when cycled in unbuffered aqueous Li_2SO_4 (pH ~ 3.5) the pseudocapacitance fades into the double-layer capacitance background over the first 100 cycles, whereas stable cycling (tested to 1000 cycles) is observed when a borate-based buffer is added to the electrolyte to bring the pH to ~8.5.[24]

Ruthenium Oxide. Ruthenium dioxide (RuO_2) is the performance champion among the pseudocapacitive metal oxides used for ECs. The specific capacitance of RuO_2 is structure-dependent and maximizes in hydrous forms ($RuO_2 \cdot xH_2O$) that possess a nanocomposite structure of electronically conductive rutile networks interpenetrated within a disordered, proton-inserting hydrous phase.[51] Unlike MnO_2 and FeO*x*, RuO_2 is an excellent electronic conductor and even disordered $RuO_2 \cdot xH_2O$ has sufficient electronic conductivity (~1 S cm^{-1}) to support high pseudocapacitance (up to ~720 F g^{-1} for $RuO_2 \cdot 0.5H_2O$) without the need for conductive carbon.[8] For practical applications, the high cost of RuO_2 can be mitigated by dispersing the oxide on high-surface-area carbons (via sol–gel, impregnation, CVD, or electrodeposition methods), a strategy that can enhance electrochemical utilization.[18,52–54] Redox deposition is another viable approach to generate RuO_2 coatings on carbon, as first demonstrated by Pickup and coworkers, who used perruthenate (RuO_4^-) and ruthenate (RuO_4^{2-}) aqueous precursors to modify carbon fiber mats and CNTs.[55,56] When cycled in 1 M H_2SO_4, the RuO_2–CNT composites yield a maximum electrode-mass normalized specific capacitance of 231 F g^{-1} at 30 wt %

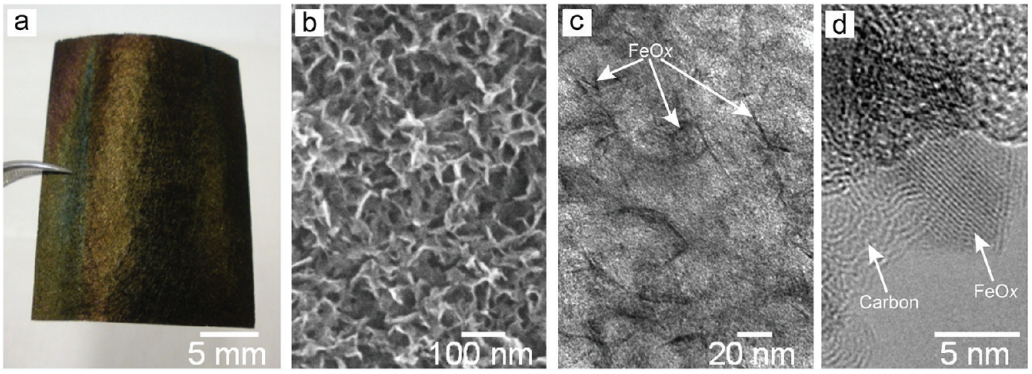

FIGURE 10. (a) Photograph, (b) scanning electron micrograph, and (c,d) transmission electron micrographs of an FeO*x*−carbon nanofoam; (d) adapted from ref 24. Copyright 2010 American Chemical Society.

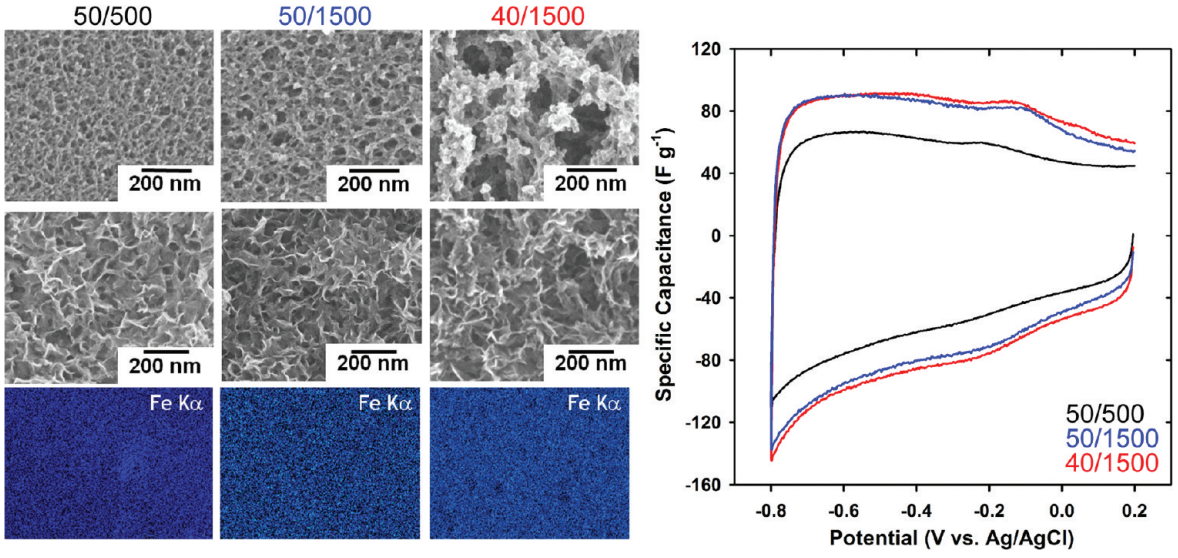

FIGURE 11. (Left) Micrographs of native carbon nanofoams (top row) and the corresponding FeO*x*−carbon nanofoams (middle row) with Fe elemental maps (bottom row). (Right) Specific capacitance versus potential for FeO*x* coatings on 50/500 (black), 50/1500 (blue), and 40/1500 (red) carbon nanofoams in 2.5 M Li_2SO_4 at 5 mV s^{-1}.

TABLE 2. Summary of Physicochemical and Electrochemical Properties of Native and FeO*x*-Coated Carbon Nanofoams

carbon nanofoam[a]	BET surface area (m^2 g^{-1})[b]	mean pore size (nm)[b]	FeO*x* wt loading (%)[c]	specific capacitance (F g^{-1})[d]	geometric capacitance (F cm^{-2})[d]	volumetric capacitance (F cm^{-3})[d]
50/500	533	9	25	54	0.28	40
50/1500	486	20	38	75	0.71	71
40/1500	332	50	38	77	0.61	61

[a]Nanofoam designations taken from the polymer nanofoam precursor formulation: e.g., "50/500" denotes a carbon nanofoam derived from 50 wt % total resorcinol−formaldehyde concentration and a resorcinol-to-catalyst (Na_2CO_3) molar ratio of 500:1. [b]Derived from N_2-sorption porosimetry for native carbon nanofoam (prior to FeO*x* deposition). [c]Determined gravimetrically. [d]Derived from cyclic voltammetric measurements at 5 mV s^{-1} in 2.5 M Li_2SO_4.

RuO_2, with up to 704 F $g_{(RuO_2)}^{-1}$ but only at lower oxide loadings (25 wt %).

Ruthenium tetroxide (RuO_4) is a related RuO_2 precursor that is better known as a staining agent for organic and biological samples in electron microscopy.[57] This precursor is commercially available as a dilute aqueous solution (0.1 wt %) with a relatively long shelf life and can be readily synthesized by oxidation of lower-valent ruthenium compounds. Ruthenium oxide deposition onto carbon substrates can be performed from either aqueous or nonaqueous RuO_4 solutions, but we find that the best results are achieved when using nonaqueous solvents. In the latter case, aqueous RuO_4 is first extracted into a hydrocarbon solvent that is cooled to dry ice−acetone bath temperatures

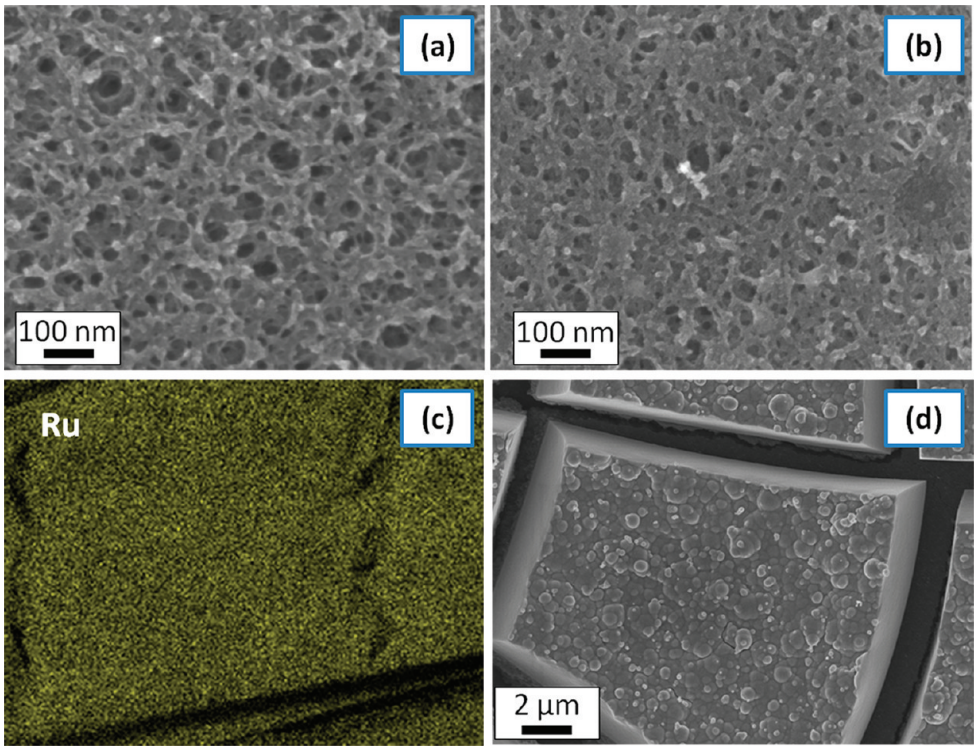

FIGURE 12. Scanning electron micrographs of a 50/1500 nanofoam: (a) before modification, (b) after RuO_2 deposition out of RuO_4–petroleum ether with (c) corresponding Ru elemental map; (d) RuO_2 crust that formed at surface of carbon nanofoam paper out of aqueous RuO_4.

(−78 °C)[58−60] prior to introducing the desired carbon substrate; RuO_2 forms spontaneously at the carbon surfaces as the solution warms to room temperature (Figure 12a–c).

The weight loading of RuO_2 depends not only on the RuO_4 concentration and deposition time, but also on the pore structure of the nanofoam; for example, a predominantly mesoporous nanofoam paper (designated 50/1500) with specific surface area of ∼450 $m^2\ g^{-1}$ supports 29 wt % RuO_2, while a macroporous nanofoam paper (designated 40/1500) of lower surface area (350 $m^2\ g^{-1}$) incorporates 16 wt % RuO_2. Alternatively, RuO_2 deposition can be performed directly from aqueous RuO_4, but the deposition is less well-controlled. Although similar RuO_2 weight loadings are achieved (30 wt %), the oxide is localized as a micrometer-thick crust at the outer boundary of the nanofoam paper (Figure 12d). The more uniform RuO_2 deposition observed using a nonaqueous solution is assisted by infiltration into the pore structure of the hydrophobic carbon nanofoam.

The pseudocapacitance of the RuO_2 coating provides a >4-fold increase in specific capacitance relative to the native nanofoam when cycled in an acidic electrolyte (Figure 13). The enhancement in capacitance tracks the RuO_2 loading, with total electrode-mass-normalized capacitances of 250 and 140 F g^{-1} for 29 wt % and 16 wt % RuO_2–nanofoam composites, respectively. The oxide-normalized capacitances (860 and 940 F $g_{(RuO_2)}^{-1}$; Figure 13b) exceed that previously reported for unsupported $RuO_2 \cdot 0.5H_2O$ (720 F g^{-1}).[8] Although derived from a nominally anhydrous synthesis, these RuO_2 coatings exhibit pseudocapacitance on par with the best hydrous ruthenium oxide, as was previously noted when using the same deposition protocol to coat silica fiber-paper substrates.[59,60] The amplification of electrode capacitance is lower when RuO_2 is expressed as a >1 μm thick crust on the nanofoam paper: capacitance decreases to 400 F $g_{(RuO_2)}^{-1}$ (corresponding to 120 F g^{-1} total electrode), indicating poorer electrochemical utilization (Figure 13b).

Applying Metal Oxide–Carbon Electrode Architectures to High-Performance Electrochemical Capacitors

The metal oxide–carbon electrode materials described above express pseudocapacitance-enhanced charge-storage functionality in nanostructured forms that, when used in asymmetric EC devices, yield attractive combinations of energy and power in conjunction with the cost and safety advantages of aqueous electrolytes.[9,12] Asymmetric

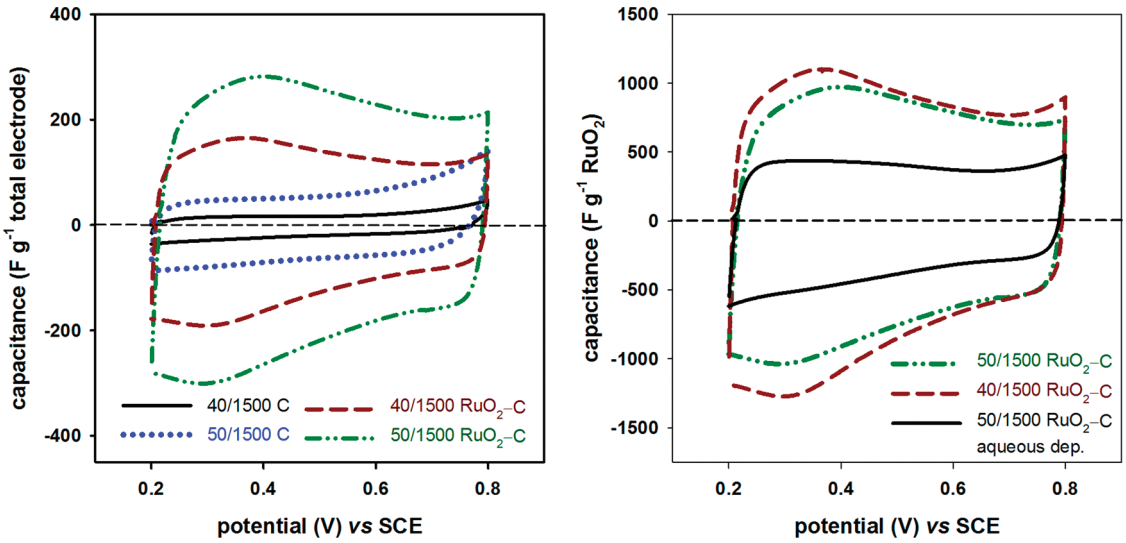

FIGURE 13. Cyclic voltammograms in 0.5 M H_2SO_4 at 2 mV s^{-1} for (left) native and RuO_2-coated nanofoams of varying pore structure; (right) comparison of RuO_2-modified nanofoams derived from either aqueous or nonaqueous RuO_4.

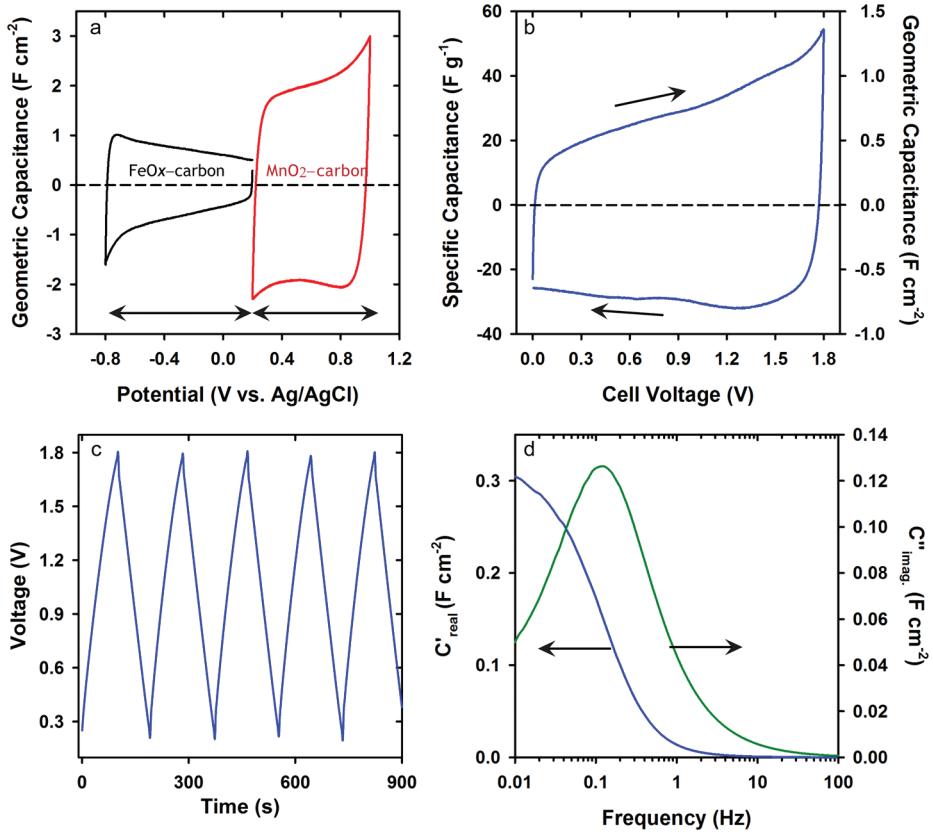

FIGURE 14. (a) Geometric capacitance versus potential for 2-ply FeO*x*– (black) and 1-ply MnO_2–carbon nanofoams; (b) specific capacitance versus potential at 5 mV s^{-1} for a full cell EC comprised of (+)1-ply MnO_2–carbon nanofoam and a (–)2-ply FeO*x*–carbon nanofoam electrode with a 25-μm Celgard-3401 separator and 2.5 M Li_2SO_4; (c) galvanostatic charge–discharge curves of the same full cell EC at 500 mA g^{-1}; (d) Bode plot of real (blue) and imaginary (green) components of capacitance versus frequency of the same full cell at 0 V.

ECs comprising a MnO_2-based positive electrode and an activated carbon negative electrode support extended operating voltages (>1.8 V) in aqueous electrolytes,[61–63] but the specific energy of this EC configuration is ultimately limited by the modest double-layer capacitance of carbon electrodes in mild-pH electrolytes (typically <120 F g^{-1}).[64]

To circumvent this limitation, one may exploit pseudocapacitance at the negative electrode to enhance specific energy using materials (e.g., poly(3,4-ethylenedioxythiophene),[65] SnO_2,[66] or FeO*x*[48,67]) whose redox-active potential window complements that of MnO_2 (see Figure 14a).

We target higher specific energy by fabricating asymmetric ECs comprising MnO_2- and FeO*x*-modified carbon nanofoams serving as positive and negative electrodes, respectively, both synthesized via the redox deposition process. The serial pairing of two pseudocapacitive electrodes yields a capacitor-like voltammetric response for the full cell (Figure 14b), but over a range of wider voltage (0−1.8 V) than obtainable by the individual electrodes. Asymmetric ECs are more complicated to design than symmetric EDLCs because care must be taken to balance the capacitance and active potential range of the opposing electrodes to realize the widest voltage window and best cycle life.[68,69] When using nanofoam papers, thickness can be increased as necessary (Figure 9) to offset lower capacitance in one of the two electrodes in order to achieve a capacity-balanced cell. For example, we compensate for the lower oxide loadings and correspondingly lower capacitance of FeO*x*−carbon nanofoams relative to their MnO_2−carbon counterparts, by using 2-ply (120 μm) versus 1-ply (70 μm) papers, respectively, when assembling the EC cell.

Even at modest oxide loadings (50 wt % MnO_2 and 20 wt % FeO*x*) and imperfect balance of positive and negative electrode capacitance (Figure 14a), cell-level performance metrics are promising, with electrode mass-, volume-, and footprint-normalized capacitances of 30 F g^{-1}, 30 F cm^{-3}, and 0.74 F cm^{-2}, respectively (not accounting for electrolyte, separator, or current collectors). Separate galvanostatic charge−discharge experiments (Figure 14c) yield 33 F g^{-1} at an imposed current of 500 mA g^{-1} (12.5 mA cm^{-2}), corresponding to a cell specific energy of 13 W h kg^{-1} at a specific power of 490 W kg^{-1}. For comparison, Brousse et al. report 8.2 W h kg^{-1} at a similar current density (450 mA g^{-1}) for a (+)MnO_2||Fe_3O_4(−) asymmetric EC assembled from composite electrodes comprising discrete oxide (at higher oxide loadings of 65−70 wt %) and carbon powders cemented together with polymer binder.[48]

The enhanced specific energy for ECs fabricated with nanofoam-based electrodes is deliverable within the few-seconds charge−discharge response times (a 9 s time constant in the example presented; see Figure 14d) that are critical for many of the proposed applications of ECs. To further underscore the ability of these design principles to amplify specific energy without compromising specific power, we contrasted the effect of pairing a MnO_2−carbon nanofoam paper with either an EDLC negative electrode (unmodified carbon nanofoam paper) or FeO*x*-painted carbon nanofoam paper. Adding the pseudocapacitive FeO*x* coating to the negative-electrode nanofoam more than doubles the specific energy while retaining specific power at ~0.5 kW kg^{-1} at 0.5 mA g^{-1}.

Future Opportunities

The pieces are now in place to design ECs with the desired specific energy, specific power, and frequency response to meet the particular performance requirements of the power/energy-demanding application. The performance of our lab-scale aqueous asymmetric ECs are already competitive with commercial nonaqueous EDLCs, and the low-cost and scalability of redox-based deposition of EC-relevant metal oxides should move these materials and structures from laboratory curiosity to real-world applications. We anticipate further advances in electrochemical performance as the metal-oxide composition, quality of contact of nanoscale metal oxide to its carbon scaffold, and micro/macroscale architecture of the electrode are fine-tuned to fully exploit the benefits of pseudocapacitance in technologically relevant form factors. Metal oxide-decorated carbon nanofoams provide important insights into the design and fabrication of EC electrode architectures, but represent only one possible device-ready electrode structure. The lessons learned with these scalable, manufacturable, benchtop-fabricated nanofoam papers can be extended to alternative free-standing carbon architectures (e.g., vertically aligned CNT assemblies)[17] that are readily adaptable to EC configurations.

We acknowledge the financial support of the U.S. Office of Naval Research.

BIOGRAPHICAL INFORMATION

Jeffrey Long is a staff scientist in the Surface Chemistry Branch at the NRL where his research centers on the development of nanostructured materials for electrochemical power sources and separation/filtration. He received a Ph.D. in Chemistry from the University of North Carolina in 1997 and a B.S. from Wake Forest University in 1992.

Megan Sassin is a Karle Fellow and staff scientist at the NRL; her research interests focus on 3D architectures for electrochemical energy storage. She received her Ph.D. from the University of California, Irvine in 2007 and B.S. from Southwestern University (2001). She was named a 2012 "Rising Star" by the American Chemical Society.

Christopher Chervin is a staff scientist at the NRL, where his research focuses on redesigning cathodes for metal−air batteries and exploring the uses of ultrathin RuO_2 films as catalytic and transparent conducting substrates. He received his Ph.D. from the University of California, Davis in 2005 and B.S. from Humboldt State University (2000).

Debra Rolison heads the Advanced Electrochemical Materials section at the NRL where she and her team design and create multifunctional nanoarchitectures for rate-critical applications, including energy storage and conversion. She received the 2011 ACS Award in the Chemistry of Materials and is a Fellow of the AAAS, MRS, ACS, and AWIS.

FOOTNOTES

*To whom correspondence should be addressed. Fax 202-767-3321. E-mail: jeffrey.long@nrl.navy.mil.

REFERENCES

1 Miller, J. R.; Burke, A. F. Electrochemical capacitors: Challenges and opportunities for real-world applications. *Interface* **2008**, *17* (1), 53–57.

2 Burke, A. Ultracapacitor technologies and application in hybrid and electric vehicles. *Int. J. Energy Res.* **2010**, *34*, 133–151.

3 Simon, P.; Burke, A. Nanostructured carbons: Double-layer capacitance and more. *Interface* **2008**, *17* (1), 38–42.

4 Simon, P.; Gogotsi, Y. Materials for electrochemical capacitors. *Nat. Mater.* **2008**, *7*, 845–854.

5 Conway, B. E.; Birss, V.; Wojtowicz, J. The role and utilization of pseudocapacitance for energy storage by supercapacitors. *J. Power Sources* **1997**, *66*, 1–14.

6 Conway, B. E.; Pell, W. G. Double-layer and pseudocapacitance types and their application to the development of hybrid devices. *J. Solid State Electrochem.* **2003**, *7*, 637–644.

7 Zhao, X.; Sánchez, B. M.; Dobson, P. J.; Grant, P. S. The role of nanomaterials in redox-based supercapacitors for next-generation energy storage devices. *Nanoscale* **2011**, *3*, 839–855.

8 Zheng, J. P.; Cygan, P. J.; Jow, T. R. Hydrous ruthenium oxide as an electrode material for electrochemical capacitors. *J. Electrochem. Soc.* **1995**, *142*, 2699–2703.

9 Bélanger, D.; Brousse, T.; Long, J. W. Manganese oxides: Battery materials make the leap to electrochemical capacitors. *Interface* **2008**, *17* (1), 49–52.

10 Wei, W.; Cui, X.; Chen, W.; Ivey, D. G. Manganese oxide-based materials as electrochemical supercapacitor electrodes. *Chem. Soc. Rev.* **2011**, *40*, 1697–1721.

11 Zhang, S. W.; Chen, G. Z. Manganese oxide-based materials for supercapacitors. *Energy Mater.* **2008**, *3*, 186–200.

12 Long, J. W.; Bélanger, D.; Brousse, T.; Sugimoto, W.; Sassin, M. B.; Crosnier, O. Asymmetric electrochemical capacitor−Stretching the limits of aqueous electrolytes. *MRS Bull.* **2011**, *36*, 513–522.

13 Rolison, D. R.; Long, J. W.; Lytle, J. C.; Fischer, A. E.; Rhodes, C. P.; Bourg, M. E.; Lubers, A. M. Multifunctional 3D nanoarchitectures for energy storage and conversion. *Chem. Soc. Rev.* **2009**, *38*, 226–252.

14 Pang, S.-C.; Anderson, M. A.; Chapman, T. W. Novel electrode materials for thin-film ultracapacitors: Comparison of electrochemical properties of sol−gel-derived and electrodeposited manganese dioxide. *J. Electrochem. Soc.* **2000**, *147*, 444–450.

15 Toupin, M.; Brousse, T.; Bélanger, D. Charge storage mechanism of MnO_2 electrode used in aqueous electrochemical capacitor. *Chem. Mater.* **2004**, *16*, 3184–3190.

16 Lee, H. Y.; Goodenough, J. B. Supercapacitor behavior with KCl electrolyte. *J. Solid State Chem.* **1999**, *144*, 220–223.

17 Zhang, H.; Cao, G. P.; Wang, Z. Y.; Yang, Y. S.; Shi, Z. J.; Gu, Z. N. Growth of manganese oxide nanoflowers on vertically-aligned carbon nanotubes arrays for high-rate electrochemical capacitive energy storage. *Nano Lett.* **2008**, *8*, 2664–2668.

18 Miller, J. M.; Dunn, B. Morphology and electrochemistry of ruthenium/carbon aerogel nanostructures. *Langmuir* **1999**, *15*, 799–806.

19 Cui, X. W.; Hu, F. P.; Wei, W. F.; Chen, W. X. Dense and long carbon nanotubes arrays decorated with Mn_3O_4 nanoparticles for electrodes of electrochemical supercapacitors. *Carbon* **2010**, *49*, 1225–1234.

20 Lin, C. K.; Wu, C. H.; Tsai, C. Y.; Chen, C. Y.; Wang, S. C. Pseudocapacitive performance of hybrid manganese oxide films with multiwalled-CNT additions. *Surf. Coat. Technol.* **2010**, *205*, 1595–1598.

21 Wu, M.; Snook, G. A.; Chen, G. Z.; Fray, D. J. Redox deposition of manganese oxide on graphite for supercapacitors. *Electrochem. Commun.* **2004**, *6*, 499–504.

22 Fischer, A. E.; Pettigrew, K. A.; Rolison, D. R.; Stroud, R. M.; Long, J. W. Incorporation of homogeneous nanoscale MnO_2 within ultraporous carbon structures via self-limiting electroless deposition: implications for electrochemical capacitors. *Nano Lett.* **2007**, *7*, 281–286.

23 Fischer, A. E.; Saunders, M. P.; Pettigrew, K. A.; Rolison, D. R.; Long, J. W. Electroless deposition of nanoscale MnO_2 on ultraporous carbon nanoarchitectures: correlation of evolving pore−solid structure and electrochemical performance. *J. Electrochem. Soc.* **2008**, *155*, A246–A252.

24 Sassin, M. B.; Mansour, A. N.; Pettigrew, K. A.; Rolison, D. R.; Long, J. W. Electroless deposition of conformal nanoscale iron oxide carbon nanoarchitectures for electrochemical charge storage. *ACS Nano* **2010**, *4*, 4505–4514.

25 Ladbury, J. W.; Cullis, C. F. Kinetics and mechanism of oxidation by permanganate. *Chem. Rev.* **1958**, *58*, 403–438.

26 Waldemer, R. H.; Tratnyek, P. G. Kinetics of contaminant degradation by permanganate. *Environ. Sci. Technol.* **2006**, *40*, 1055–1061.

27 Bach, S.; Henry, M.; Baffier, N.; Livage, J. Sol−gel synthesis of manganese oxides. *J. Solid State Chem.* **1990**, *88*, 325–333.

28 Ching, S.; Landrigan, J. A.; Jorgensen, M. L.; Duan, N.; Suib, S. L. Sol−gel synthesis of birnessite from $KMnO_4$ and simple sugars. *Chem. Mater.* **1995**, *7*, 1604–1606.

29 Ma, S. B.; Lee, Y.-H.; Ahn, K.-Y.; Kim, C.-M.; Oh, K.-H.; Kim, K.-B. Spontaneously deposited manganese oxide on acetylene black in an aqueous potassium permanganate solution. *J. Electrochem. Soc.* **2006**, *153*, C27–C32.

30 Huang, X.; Yue, H.; Attia, A.; Yang, Y. Preparation and properties of manganese oxide/carbon composites by reduction of potassium permanganate with acetylene black. *J. Electrochem. Soc.* **2007**, *154*, A26–A33.

31 Dong, X.; Shen, W.; Gu, J.; Xiong, L.; Zhu, Y.; Li, H.; Shi, J. A structure of MnO_2 embedded in CMK-3 framework developed by a redox method. *Microporous Mesoporous Mater.* **2006**, *91*, 120–127.

32 Dong, X.; Shen, W.; Gu, J.; Xiong, L.; Zhu, Y.; Li, H.; Shi, J. MnO_2-embedded-in-mesoporous-carbon-wall structure for use as electrochemical capacitors. *J. Phys. Chem. B* **2006**, *110*, 6015–6019.

33 Patel, M. N.; Wang, X.; Wilson, B.; Ferrer, D. A.; Dai, S.; Stevenson, K. J.; Johnston, K. P. Hybrid MnO_2-disordered mesoporous carbon nanocomposites: synthesis and characterization as electrochemical pseudocapacitor electrodes. *J. Mater. Chem.* **2010**, *20*, 390–398.

34 Peng, Y.; Chen, Z.; Wen, J.; Xiao, C.; Weng, D.; He, S.; Geng, H.; Lu, Y. Hierarchical mangananse oxide/carbon nanocomposites for supercapacitor electrodes. *Nano Res.* **2011**, *4*, 216–225.

35 Jin, X.; Zhou, W.; Zhang, S.; Chen, G. Z. Nanoscale microelectrochemical cells on carbon nanotubes. *Small* **2007**, *9*, 1513–1517.

36 Ma, S.-B.; Ahn, K.-Y.; Lee, E.-S.; Oh, K.-H.; Kim, K.-B. Synthesis and characterization of manganese dioxide spontaneously coated on carbon nanotubes. *Carbon* **2007**, *45*, 375–382.

37 Chu, H.-Y.; Lai, Q.-Y.; Wang, L.; Lu, J.-F.; Zhao, Y. Preparation of MnO_2/WMNT composite and MnO_2/AB composite by redox deposition method and its comparative study as supercapacitive materials. *Ionics* **2010**, *16*, 233–238.

38 Zhang, S.; Peng, C.; Ng, K. C.; Chen, G. Z. Nanocomposites of manganese oxides and carbon nanotubes for aqueous supercapacitor stacks. *Electrochim. Acta* **2010**, *55*, 7447–7453.

39 Bordjiba, T.; Bélanger, D. Direct redox deposition of manganese oxide on multiscaled carbon nanotube/microfiber carbon electrode for electrochemical capacitor. *J. Electrochem. Soc.* **2009**, *156*, A378–A384.

40 Bordjiba, T.; Bélanger, D. Development of new nanocomposite based on nanosized-manganese oxide and carbon nanotubes for high performance electrochemical capacitors. *Electrochim. Acta* **2010**, *55*, 3428–3433.

41 Yan, J.; Fan, Z.; Wei, T.; Qian, W.; Zhang, M.; Wei, F. Fast and reversible surface redox reaction of graphene-MnO_2 composites as supercapacitor electrodes. *Carbon* **2010**, *48*, 3825–3833.

42 Wang, L.; Wang, D.-L. Preparation and electrochemical characterization of MnOOH nanowire-graphene oxide. *Electrochim. Acta* **2011**, *56*, 5010–5015.

43 Perez-Bentio, J. F.; Arias, C.; Brillas, E. A kinetic study of the autocatalytic permanganate oxidation of formic acid. *Int. J. Chem. Kinet.* **1990**, *22*, 261–287.

44 Pekala, R. W.; Farmer, J. C.; Alviso, C. T.; Tran, T. D.; Mayer, S. T.; Miller, J. M.; Dunn, B. Carbon aerogels for electrochemical applications. *J. Non-Cryst. Solids* **1998**, *225*, 74–80.

45 Lytle, J. C.; Wallace, J. M.; Sassin, M. B.; Barrow, A. J.; Long, J. W.; Dysart, J. L.; Renninger, C. H.; Saunders, M. P.; Brandell, N. L.; Rolison, D. R. The right kind of interior for multifunctional electrode architectures: carbon nanofoam papers with aperiodic submicrometer pore networks interconnected in 3D. *Energy Environ. Sci.* **2011**, *4*, 1913–1925.

46 Sharma, V. K. Potassium ferrate(VI): An environmentally friendly oxidant. *Adv. Environ. Res.* **2002**, *6*, 143–156.

47 Mao, W.; Wang, J.; Xu, Z.; Niu, Z.; Zhang, J. Effects of the oxidation treatment with K_2FeO_4 on the physical properties and electrochemical performance of a natural graphite as electrode material for lithium ion batteries. *Electrochem. Commun.* **2006**, *8*, 1326–1330.

48 Brousse, T.; Bélanger, D. Hybrid Fe_3O_4-MnO_2 capacitor in mild aqueous electrolyte. *Electrochem. Solid-State Lett.* **2003**, *6*, A244–A248.

49 Chung, K. W.; Kim, K. B.; Han, S.-H. Novel synthesis and electrochemical characterization of nano-sized cellular Fe_3O_4 thin film. *Electrochem. Solid-State Lett.* **2005**, *8*, A259–A262.

50 Wu, M.-S.; Lee, R.-H.; Jow, J.-J.; Yang, W.-D.; Hsieh, C.-Y.; Weng, B.-J. Nanostructured iron oxide films prepared by electrochemical method for electrochemical capacitors. *Electrochem. Solid-State Lett.* **2009**, *12*, A1–A4.

51 Dmowski, W.; Egami, T.; Swider-Lyons, K. E.; Love, C. T.; Rolison, D. R. Local atomic structure and conduction mechanism of nanocrystalline hydrous RuO_2 from X-ray scattering. *J. Phys. Chem. B* **2002**, *106*, 12677–12683.

52 Hu, C. C.; Chen, W. C.; Chang, K. H. How to achieve maximum utilization of hydrous ruthenium oxide for supercapacitors. *J. Electrochem. Soc.* **2005**, *151*, A281–A290.

53 Kim, I. H.; Kim, J. H.; Lee, Y. H.; Kim, K. B. Synthesis and characterization of electrochemically prepared ruthenium oxide on carbon nanotube film substrate for supercapacitor application. *J. Electrochem. Soc.* **2005**, *152*, A2170–A2178.

54 Panic, V. V.; Dekanski, A. B.; Stevanovic, R. M. Sol−gel processed thin-layer ruthenium oxide/carbon black supercapacitors: A revelation of the energy storage issues. *J. Power Sources* **2010**, *195*, 3969–3976.

55 Liu, X.; Huber, T. A.; Kopac, M. C.; Pickup, P. G. Ru oxide/carbon nanotubes composites for supercapacitors prepared by spontaneous reduction of Ru(VI) and Ru(VII). *Electrochim. Acta* **2009**, *54*, 7141–7147.

56 Liu, X.; Pickup, P. G. Carbon fabric supported manganese and ruthenium oxide thin films for supercapacitors. *J. Electrochem. Soc.* **2011**, *158*, A241–A249.

57 Trent, J. S.; Scheinbeim, J. I.; Couchman, P. R. Ruthenium tetraoxide staining of polymers for electron microscopy. *Macromolecules* **1983**, *16*, 589–598.

58 Ryan, J. V.; Berry, A. D.; Anderson, M. L.; Long, J. W.; Stroud, R. M.; Cepak, V. M.; Browning, V. M.; Rolison, D. R.; Merzbacher, C. I. Electronic connection to the interior of a mesoporous insulator with nanowires of crystalline RuO_2. *Nature* **2000**, *406*, 169–172.

59 Chervin, C. N.; Lubers, A. M.; Pettigrew, K. A.; Long, J. W.; Westgate, M. A.; Fontanella, J. J.; Rolison, D. R. Making the most of a scarce platinum-group metal: Conductive ruthenia nanoskins on insulating silica paper. *Nano Lett.* **2009**, *9*, 2316–2321.

60 Chervin, C. N.; Lubers, A. M.; Long, J. W.; Rolison, D. R. Effect of temperature and atmosphere on the conductivity and electrochemical capacitance of single-unit-thick ruthenium dioxide. *J. Electroanal. Chem.* **2010**, *644*, 155–163.

61 Hong, M. S.; Lee, S. H.; Kim, S. W. The use of KCl electrolyte for 2 V manganese oxide/activated carbon hybrid capacitor. *Electrochem. Solid State Lett.* **2002**, *5*, A227–A230.

62 Khomenko, V.; Raymundo-Piñero, E.; Béguin, F. Optimisation of an asymmetric manganese oxide/activated carbon capacitor working at 2 V in aqueous medium. *J. Power Sources* **2006**, *153*, 183–190.

63 Brousse, T.; Taberna, P.-L.; Crosnier, O.; Dugas, R.; Guillemet, P.; Scudeller, Y.; Zhou, Y.; Favier, F.; Bélanger, D.; Simon, P. Long-term cycling behavior of asymmetric activated carbon/MnO_2 aqueous electrochemical supercapacitor. *J. Power Sources* **2007**, *173*, 633–641.

64 Andreas, H. A.; Conway, B. E. Examination of the double-layer capacitance of an high specific-area C-cloth electrode as titrated from acidic to alkaline pHs. *Electrochim. Acta* **2006**, *51*, 6510–6520.

65 Khomenko, V.; Raymundo-Piñero, E.; Frackowiak, E.; Béguin, F. High-voltage asymmetric supercapacitors operating in aqueous electrolyte. *Appl. Phys. A: Mater. Sci. Process.* **2006**, *82*, 567–573.

66 Ng, K. C.; Zhang, S.; Peng, C.; Chen, G. Z. Individual and bipolarly stacked asymmetrical aqueous supercapacitors of CNTs/SnO_2 and CNTs/MnO_2 nanocomposites. *J. Electrochem. Soc.* **2009**, *156*, A846–A853.

67 Jin, W.-H.; Cao, G.-T.; Sun, J.-Y. Hybrid supercapacitor based on MnO_2 and columned FeOOH using Li_2SO_4 electrolyte solution. *J. Power Sources* **2008**, *175*, 686–691.

68 Li, J.; Gao, F. Analysis of electrodes matching for asymmetric electrochemical capacitor. *J. Power Sources* **2009**, *194*, 1184–1193.

69 Demarconnay, L; Raymundo-Piñero, E.; Béguin, F. Adjustment of electrodes potential window in an asymmetric carbon/MnO_2 supercapacitor. *J. Power Sources* **2011**, *196*, 580–586.